

Nanoscale Packing Differences in Sphingomyelin and Phosphatidylcholine Revealed by BODIPY Fluorescence in Monolayers: Physiological Implications

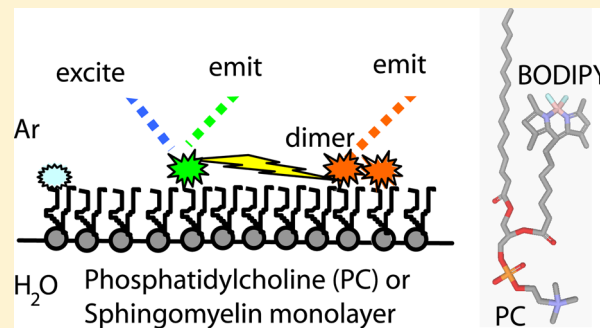
Xiuhong Zhai,[†] Ivan A. Boldyrev,[‡] Nancy K. Mizuno,[†] Maureen M. Momsen,[†] Julian G. Molotkovsky,^{*,‡} Howard L. Brockman,^{*,†} and Rhoderick E. Brown^{*,†}

[†]Hormel Institute, University of Minnesota, 801 16th Ave NE, Austin, Minnesota 55912, United States

[‡]Shemyakin-Ovichinnikov Institute of Bioorganic Chemistry, Russian Academy of Sciences, Moscow, Russian Federation

Supporting Information

ABSTRACT: Phosphatidylcholines (PC) with two saturated acyl chains (e.g., dipalmitoyl) mimic natural sphingomyelin (SM) by promoting raft formation in model membranes. However, sphingoid-based lipids, such as SM, rather than saturated-chain PCs have been implicated as key components of lipid rafts in biomembranes. These observations raise questions about the physical packing properties of the phase states that can be formed by these two major plasma membrane lipids with identical phosphocholine headgroups. To investigate, we developed a monolayer platform capable of monitoring changes in surface fluorescence by acquiring multiple spectra during measurement of a lipid force–area isotherm. We relied on the concentration-dependent emission changes of 4,4-difluoro-4-bora-3a,4a-diaza-s-indacene (BODIPY)-labeled PC to detect nanoscale alterations in lipid packing and phase state induced by monolayer lateral compression. The BODIPY-PC probe contained an indacene ring with four symmetrically located methyl (Me) substituents to enhance localization to the lipid hydrocarbon region. Surface fluorescence spectra indicated changes in miscibility even when force–area isotherms showed no deviation from ideal mixing behavior in the surface pressure versus cross-sectional molecular area response. We detected slightly better mixing of Me₄-BODIPY-8-PC with the fluid-like, liquid expanded phase of 1-palmitoyl-2-oleoyl-PC compared to N-oleoyl-SM. Remarkably, in the gel-like, liquid condensed phase, Me₄-BODIPY-8-PC mixed better with N-palmitoyl-SM than dipalmitoyl-PC, suggesting naturally abundant SMs with saturated acyl chains form gel-like lipid phase(s) with enhanced ability to accommodate deeply embedded components compared to dipalmitoyl-PC gel phase. The findings reveal a fundamental difference in the lateral packing properties of SM and PC that occurs even when their acyl chains match.



INTRODUCTION

Biomembranes contain various types of lipids characterized by subtle physicochemical differences. As a result, the lipids can self-organize into nonrandom lateral states, e.g. raft micro-domains, within membrane bilayers.^{1–4} Elucidation of the lipid structural features of lipids that regulate their lateral distributional tendencies in biomembranes has relied on model membranes, i.e., bilayer vesicles and monolayer films, where adjustments and control of lipid compositions are relatively straightforward. When the lipids contain fluorophore tracking probes, imaging by epifluorescence microscopy provides direct insights into lipid lateral organization at the micrometer level.^{5,6} This resolution enables visualization of lipid domains but inherently constrains and limits detection of microdomains. This challenge has been largely overcome by using Förster resonance energy transfer (FRET) and fluorophore quenching as well as new super-resolution fluorescence imaging approaches.^{7,8} However, technical challenges and high costs have limited application to lipid

monolayers despite inherent advantages that include lipid matrix stability over broad ranges of lipid mixing compositions and phase states.^{9–13} This experimental flexibility is poorly duplicated in bilayer model membranes where changes in lipid composition can manifest as altered mesomorphic structure of the lipid aggregate. Lipid monolayers also display almost all physical features associated with lipid bilayers^{9–12} including the liquid-ordered phase.¹⁴

In monolayers, lipid domain visualization often requires low surface pressures that result in packing conditions atypical of biomembranes. To facilitate detection of nanoscale changes in lipid packing associated with microdomain organization in lipid monolayers under biomembrane-like packing conditions, i.e. high surface pressures, we developed a monolayer platform that monitors changes in surface fluorescence by acquiring multiple

Received: December 9, 2013

Revised: January 24, 2014

Published: February 24, 2014

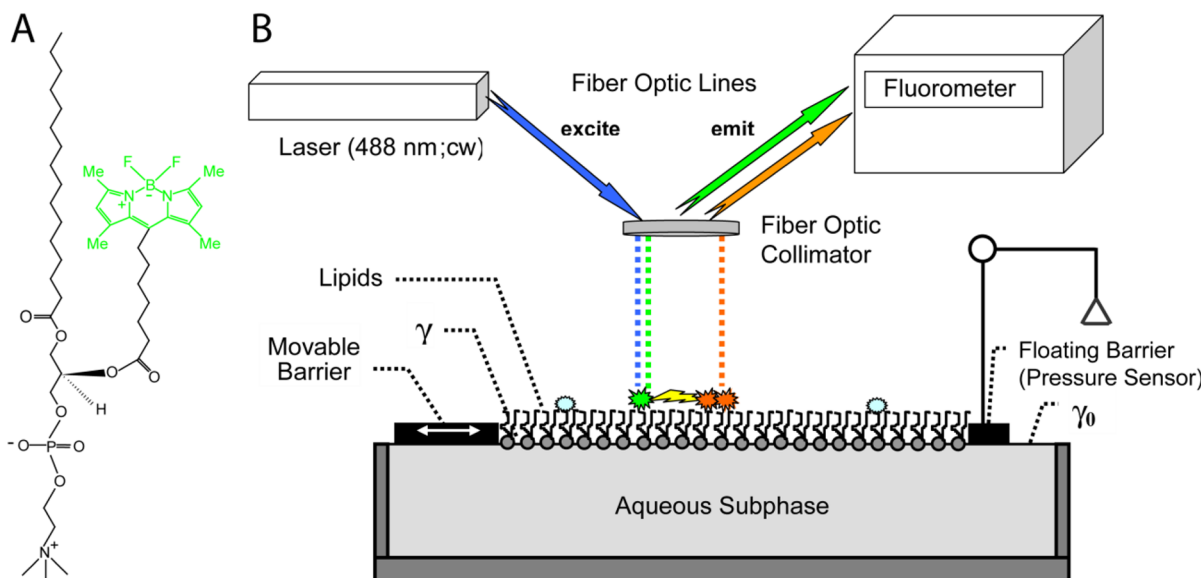


Figure 1. Langmuir surface balance modified to acquire surface fluorescence spectra of lipids forming a monolayer at the air/water interface. (A) Structure of Me₄-BODIPY-8-PC. (B) Schematic of modified Langmuir film balance equipped to acquire surface fluorescence.

spectra during measurement of a lipid force–area isotherm.^{15,16} By taking advantage of the concentration-dependent emission changes of 4,4-difluoro-4-bora-3a,4a-diaza-s-indacene (BODIPY), we could detect alterations in lipid packing density induced by lateral compression (at constant probe mole fraction) or by variation of the lipid fluorophore mole fraction in a fluid POPC monolayer, even when classic analyses of force–area isotherms indicated no deviation from ideal mixing behavior. For the study, we synthesized BODIPY containing four symmetrically located methyl substituents on an indacene ring omega-linked by ring position 8 to a fatty acid which then was used to reacylate lyso-PC.¹⁷ The net effect of these synthetic changes to BODIPY is to enhance fluorophore embedding among the lipid hydrocarbon chains and lessen fluorophore looping toward the membrane surface, as has been reported for NBD and dimethyl-BODIPY (ref 16 and references therein). With Me₄-BODIPY-8-PC, high surface concentrations produce emission peak broadening rather than a distinct, long-wavelength, excited-state, dimer peak (e.g., dimethyl-BODIPY).¹⁶ Principal Component Analysis provides a mathematical means for efficient evaluation of the hundreds of emission spectra acquired during collection of each force–area isotherm, enabling insights into lipid miscibility.¹⁸

Here we show the efficacy of this monolayer platform by addressing the following biophysics issue involving two major plasma membrane lipids containing identical phosphocholine headgroups: PC and sphingomyelin (SM). When these two glycerol-based and sphingoid-based lipids have identical acyl chains, do physical packing differences exist in the phase states that can regulate mixing behavior with other membrane components, e.g., other lipids? In naturally prevalent membrane phosphoglycerides such as PC, both hydrocarbon chains generally are ester-linked to a glycerol backbone, the *sn*-1 chain is typically saturated (e.g., palmitate or stearate), and the *sn*-2 chain contains one or more *cis* double bonds. These features keep the PC chains in a fluid state well below physiological temperatures. However, it is well-known from model membrane studies that saturation of the PC *sn*-2 chain (e.g., palmitate) raises the temperature needed for the resulting dipalmitoyl PC (DPPC) bilayers to be fluid to ~42 °C. In

membrane sphingolipids such as naturally prevalent SM, the 18-carbon sphingoid base chain serves the dual role of interfacial backbone and nonpolar hydrocarbon chain. The single acyl chain is amide-linked and typically is saturated, resulting in temperatures in the 42–46 °C range (depending on acyl composition) being needed for SM to become fluid in the bilayer state. Thus, at physiological temperature, most natural SMs are not fluid and form gel-like bilayer phases.^{19–22}

The fact that mammalian cells consume energy to produce major quantities of both PC and SM suggests their phase structures could have physical differences that warrant the presence of both lipids in specific biomembranes, extending beyond their known functions as pools for generation of differing signaling metabolites. To address the issue, we investigated the ability of BODIPY-labeled PC to reveal subtle differences in lipid phase state behavior as well as changes in the lateral interactions related to micromixing of BODIPY-PC in PC compared to SM.

MATERIALS AND METHODS

1-Palmitoyl-2-oleoyl-*sn*-glycero-3-phosphatidylcholine (POPC) and 1,2-dipalmitoylphosphatidylcholine (DPPC) were obtained from Avanti Polar Lipids (Alabaster, AL). *N*-Palmitoysphingomyelin (16:0 SM) and *N*-oleoylsphingomyelin (18:1^{Δ9(c)} SM) were produced by reacylation of lyso-SM with the desired fatty acyl residue and purified as described previously (ref 13 and references therein). 1-Palmitoyl-2-(4,4-difluoro-1,3,5,7-tetramethyl-4-bora-3a,4a-diaza-s-indacene-8-heptanoyl)-*sn*-glycero-3-phosphocholine (Me₄-BODIPY-8-PC or B-PC) was synthesized and purified as described earlier¹⁷ (Figure 1A).

Langmuir Film Balance. Figure 1B illustrates how our Langmuir film balance was outfitted for acquisition of fluorescence emission intensity as a function of wavelength while simultaneously measuring surface pressure (π) as a function of lipid cross-sectional molecular area (A) of the lipid monolayer.^{15,16} Briefly, the Langmuir film balance was fitted with fiber-optic cables and collimators using home-built attachments. An opaque, blackened box with a port for surface cleaning and sample addition covered the entire monolayer trough assembly (not shown). Incident light for excitation at 90° was provided by a 488 nm argon-ion laser (Model 2122-4SL, JDS Uniphase, San Jose, CA) equipped with a model-3 light-intensity controller and a fiber-optic coupler (Model HPUC-23-488-S-3, FAC-

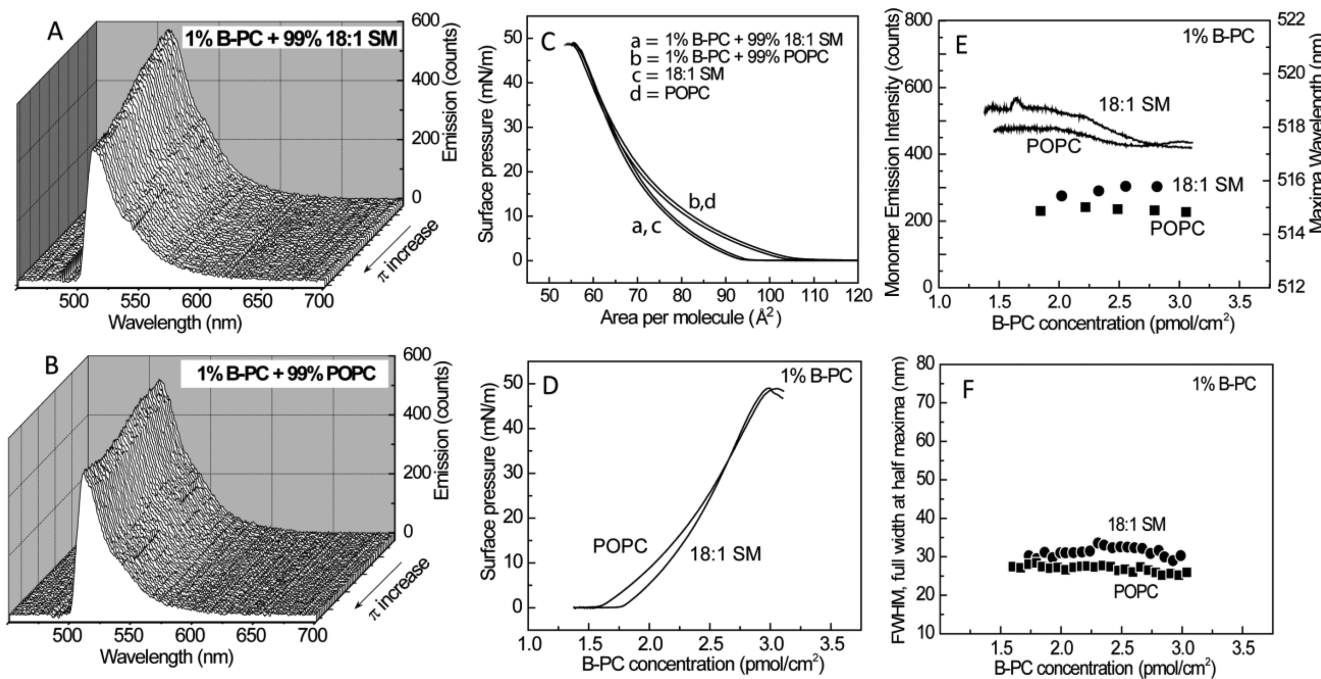


Figure 2. Compression-induced changes in fluorescence emission properties and force–area isotherms for 1 mol % $\text{Me}_4\text{-BODIPY-8-PC}$ mixed with either 18:1-SM or POPC. (A, B) Representative emission spectra obtained for mixed monolayers of 1 mol % BODIPY-PC and 18:1-SM (A) or POPC (B). (C) Monolayer isotherms for 18:1-SM and POPC showing surface pressure (π) versus average molecular area in absence and presence of lipid fluorophore. (D) Surface pressure versus BODIPY-PC surface concentration (pmol/cm^2) response. (E) Monomer emission intensity (solid line) and emission wavelength maximum (λ_{\max}) (symbol) versus BODIPY-PC surface concentration (pmol/cm^2) in 18:1-SM or POPC. The monomer emission intensity represents the integrated area over the 505–535 nm range. (F) Emission peak broadening versus BODIPY-PC surface concentration (pmol/cm^2) in 18:1-SM or POPC. The broadening represents the peak width (nm) determined at 50% maximum intensity.

2BL; Oz Optics, Nepean, ON, Canada). After exiting a collimator, the light passed through a 2° holographic diffusing filter (Coherent, Auburn, CA) and was masked to project a circular spot (~ 0.5 cm diameter) on the monolayer surface. The projected spot intensity was ~ 1.5 mW/cm 2 . Fluorescence emission was collected perpendicular to the interface at a ~ 1 cm distance using a fiber-optic spectrometer (Model PC2000-ISA, Ocean Optics, Dunedin, FL) equipped with an L2 lens and a $200\ \mu\text{m}$ slit. A 500 nm long pass filter (500EFLP, Omega Optical, Brattleboro, VT) was mounted between the emission collimator and the detector to reduce scattered excitation light. Spectra (480–700 nm) were collected using 1 s acquisition times at 2 s intervals (OOIBase32 software) during monolayer compression. The fractional change in lipid surface concentration during each spectral acquisition cycle was ≤ 0.0073 . This value was calculated by considering the (i) molecular compression rate ($\sim 4\ \text{\AA}^2/\text{molecule}/\text{min}$), (ii) original surface area of the spread lipid, and (iii) 3 s spectral acquisition cycle. Control emission spectra were unaffected by gas phase (air or argon) or by 0.01% sodium azide in the subphase buffer. Each reported isotherm is an average of at least two determinations to correct for small changes in the fiber-optical path caused by cover removal between runs.

Lipid monolayers were formed by spreading ($51\ \mu\text{L}$ aliquots) of mixtures made from stock solutions dissolved in hexane/ethanol (9:1) or hexane/isopropanol/water (70:30:2.5). The PC, SM, and $\text{Me}_4\text{-BODIPY-8-PC}$ stock concentrations were quantified by a modified Barlett assay.^{15,16} $\text{Me}_4\text{-BODIPY-8-PC}$ stock concentration also was checked by extinction coefficient ($87\ 000\ \text{M}^{-1}\ \text{cm}^{-1}$ at 505 nm). After spreading on the subphase surface and a delay period of 4 min, lipid films were compressed at a rate of $\leq 4\ \text{\AA}^2/\text{molecule}/\text{min}$ on subphase maintained at $24\ ^\circ\text{C}$ via a thermostated circulating water bath. Surface pressure and area calibration of the film balance were performed as detailed previously (ref 13 and references therein). Solvent purity was verified by dipole potential measurements using a ^{210}Po ionizing electrode (ref 13 and references therein).

Subphase buffer was produced using water purified by reverse osmosis, activated charcoal adsorption, and mixed-bed deionization, then passed through a Milli-Q UV Plus System (Millipore Corp., Bedford, MA), and filtered through a $0.22\ \mu\text{m}$ Millipak 40 membrane. Subphase buffer contained 10 mM potassium phosphate (pH 6.6), 100 mM NaCl, and 0.2% NaN_3 and was kept stored under argon. The argon was cleaned by passage through a seven-stage series filtration setup consisting of an Alltech activated charcoal gas purifier, a LabClean filter, and a series of Balston disposable filters consisting of two adsorption (carbon) and three filter units (93% and 99.99% efficiency at $0.1\ \mu\text{m}$). The film balance was housed in an isolated laboratory supplied with clean air by a Bioclean Air Filtration system equipped with charcoal and HEPA filters and was kept under humidified argon in a separate enclosure. Other features contributing to isotherm reproducibility include automated lipid spreading via a modified HPLC autoinjector, automated surface cleaning by multiple barrier sweeps between runs, and highly accurate, reproducible setting of the subphase level by an automated aspirator. Glassware was acid cleaned and rinsed with purified water and then with hexane/ethanol (95:5) before use.

RESULTS AND DISCUSSION

$\text{Me}_4\text{-BODIPY-8-PC}$, like many BODIPY probes, has high photostability, is nearly insensitive to environmental polarity, and has a small Stokes shift.¹⁶ Dilute noninteracting BODIPY monomers exhibit a narrow emission peak centered in the 506–515 nm range.^{15,16,18,26–31} At high BODIPY concentrations, a second, longer-wavelength fluorescence peak also can occur due to excited-state dimer emission. With dimethyl-BODIPY, the wavelength shift of the excited-state dimer is sufficiently strong for the peak to be resolved from its monomer emission peak.¹⁵ However, in the case of tetramethyl-BODIPY (e.g., $\text{Me}_4\text{-BODIPY-8-PC}$ is studied

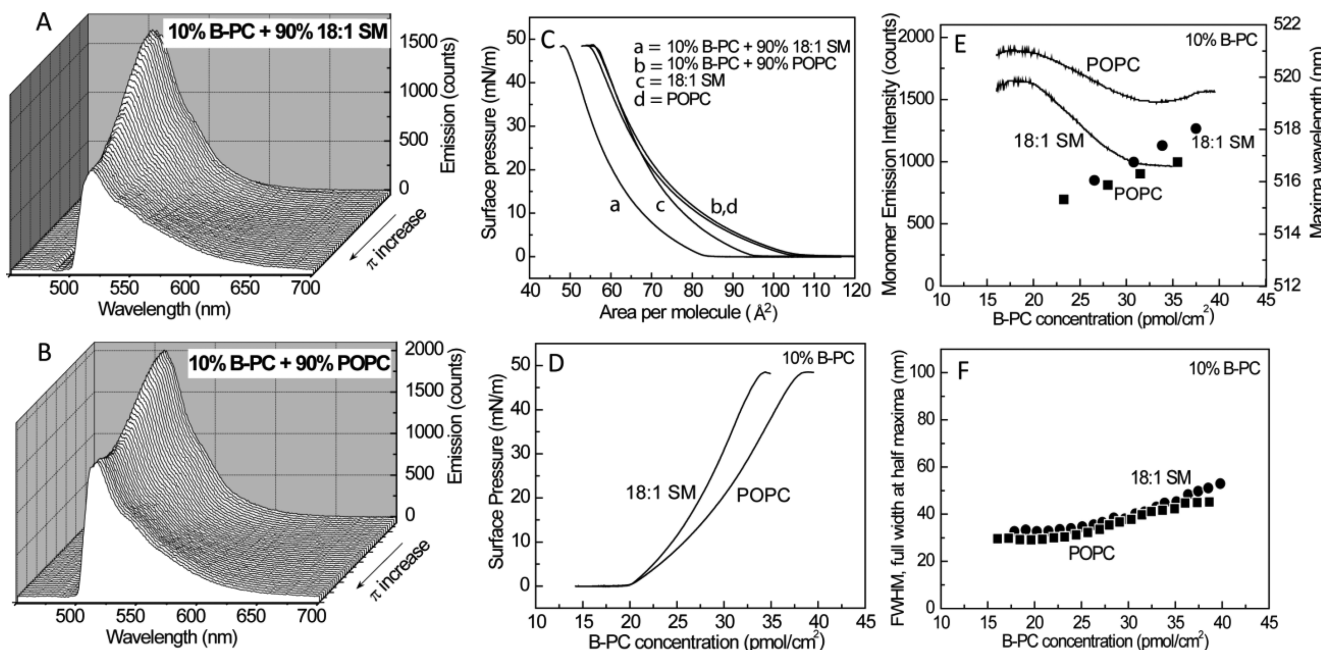


Figure 3. Compression-induced changes in fluorescence emission properties and force–area isotherms for 10 mol % $\text{Me}_4\text{-BODIPY-8-PC}$ mixed with either 18:1-SM or POPC. (A, B) Representative emission spectra obtained for mixed monolayers of 10 mol % BODIPY-PC and 18:1-SM (A) or POPC (B). (C) Monolayer isotherms for 18:1-SM and POPC showing surface pressure versus average molecular area in absence and presence of lipid fluorophore. (D) Surface pressure (π) versus BODIPY-PC surface concentration (pmol/cm^2) response. (E) Monomer emission intensity (solid line) and emission wavelength maximum (λ_{\max}) (symbol) versus BODIPY-PC surface concentration (pmol/cm^2) in 18:1-SM or POPC. The monomer emission intensity represents the integrated area over the 505–535 nm range. (F) Emission peak broadening versus BODIPY-PC surface concentration (pmol/cm^2) in 18:1-SM or POPC. The broadening represents the peak width (nm) determined at 50% maximum intensity.

here), the dimer emission peak wavelength is not shifted as much and is not distinctly resolved from the monomer peak. Also, resonance energy transfer (Förster distance = 57 Å) may contribute to excitation of transient ground state dimers, partially quenching monomer emission. The end result is spectral broadening that increases with increasing contribution from the concentration-dependent dimer emission. The preceding information is provided to facilitate understanding of the experimental data that follows.

$\text{Me}_4\text{-BODIPY-8-PC}$ Response in 18:1-Sphingomyelin Compared to POPC. We began addressing the issues (see Introduction) by evaluating the lateral mixing of $\text{Me}_4\text{-BODIPY-8-PC}$ in SM versus PC when the hydrocarbon chain structural differences controlling their phase behavior were minimal. We initially focused on 18:1-SM, which, like POPC, displays liquid-expanded (fluid-like) behavior at all surface pressures below film collapse²⁰ and collected multiple emission spectra as the monolayers were being laterally compressed (Figure 2) using 1 mol % $\text{Me}_4\text{-BODIPY-8-PC}$ in the monolayers to minimize probe effects. Samplings (~50) from the >500 spectra obtained during acquisition of each 18:1-SM and POPC force–area isotherm are shown in Figures 2A and 2B, respectively. Increasing surface pressure affects the emission intensity and peak shape of $\text{Me}_4\text{-BODIPY-8-PC}$. The emission changes primarily reflect concentration-dependent dimer emission and possibly FRET (Förster distance = 57 Å) from BODIPY-lipid monomers to transient BODIPY-lipid dimers, induced by lateral compression of the lipid films.¹⁶ The changes observed in 18:1-SM are slightly more accentuated than those of POPC monolayers containing the same lipid probe consistent with earlier findings obtained from only four spectral data sets for POPC.¹⁶ Figures 2C and 2D illustrate the relationship between surface pressure (π) and $\text{Me}_4\text{-BODIPY-8-PC}$ lateral concen-

tration, i.e. surface density, in 18:1-SM and POPC monolayers. The emission intensity of BODIPY monomer exhibits a slightly steeper decline in 18:1-SM than in POPC over same range of increasing surface density of PC-fluorophore (Figure 2E). Moreover, the emission wavelength maximum (λ_{\max}) of $\text{Me}_4\text{-BODIPY-8-PC}$ exhibits an apparent red-shift that linearly increases with increasing surface density of the PC-fluorophore in 18:1-SM monolayers while the λ_{\max} in POPC remains unchanged (Figure 2E). Red-shifting of the λ_{\max} of BODIPY-PC fluorophores in monolayers previously has been linked to lateral surface concentration.^{15,16} Finally, the emission peak broadening of $\text{Me}_4\text{-BODIPY-8-PC}$, as assessed by the peak width at half-maximal peak height (Figure 2F), remains unchanged and similar in 18:1-SM and POPC over the BODIPY-PC surface density range of 1.5–3.0 pmol/cm^2 . In general, broadening of the BODIPY emission peak originates from additional absorption and emission peaks that occur at high BODIPY concentrations reflecting dimer emission and possibly FRET from BODIPY-lipid monomers to transient BODIPY-lipid dimers.

To confirm and better define how the spectral response provides insights into mixing behavior, higher $\text{Me}_4\text{-BODIPY-8-PC}$ amounts (10 and 20 mol %) also were studied in 18:1-SM and compared with the responses observed in POPC. With both monolayer matrix lipids, peak broadening became more pronounced with increasing π (Figure 3A,B) but was more dramatic with 20 mol % probe (not shown; see ref 16). The broadening could be traced to a shoulder peak (540–585 nm) that gains prominence relative to monomer emission intensity with the higher BODIPY-PC surface concentrations as the surface pressure increases. The shoulder peak has been previously linked to excited-state dimer emission that occurs at higher BODIPY-PC surface concentrations (ref 16 and

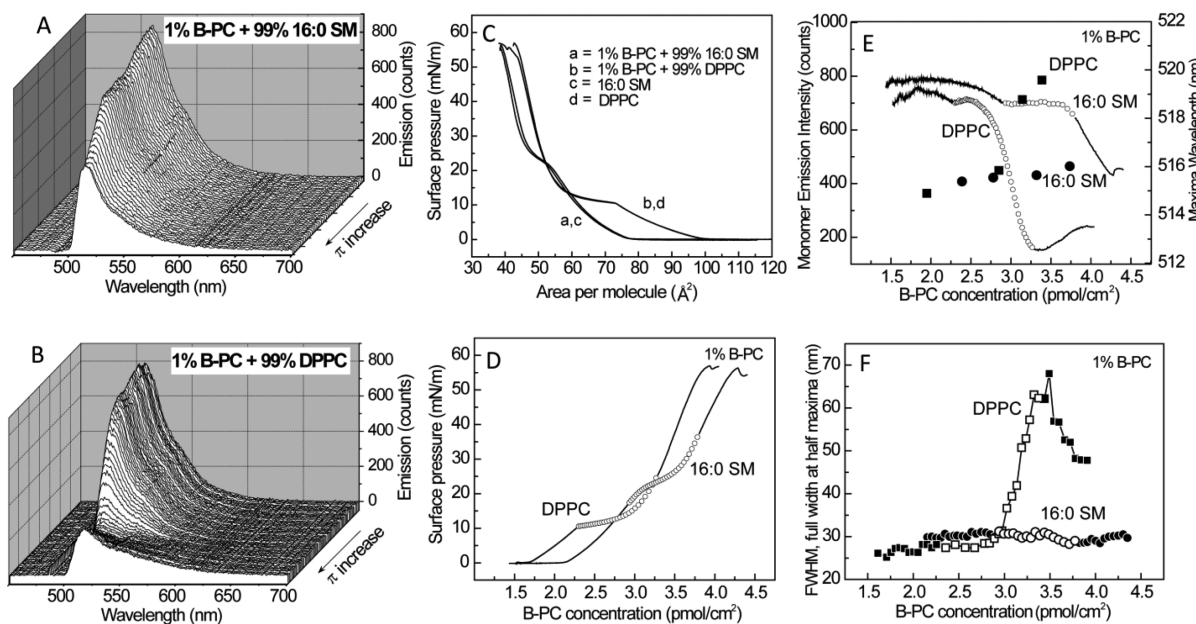


Figure 4. Compression-induced changes in fluorescence emission properties and force–area isotherms for 1 mol % $\text{Me}_4\text{-BODIPY-8-PC}$ mixed with either 16:0-SM or DPPC. (A, B) Representative emission spectra obtained for mixed monolayers of 1 mol % BODIPY-PC and 16:0-SM (A) or DPPC (B). (C) Monolayer isotherms for 16:0-SM and DPPC showing surface pressure versus average molecular area in absence and presence of lipid fluorophore. (D) Surface pressure (π) versus BODIPY-PC surface concentration (pmol/cm^2) response. (E) Monomer emission intensity (solid line) and emission wavelength maximum (λ_{\max}) (symbol) versus BODIPY-PC surface concentration (pmol/cm^2) in 16:0-SM or DPPC. The monomer emission intensity represents the integrated area over the 505–535 nm range. (F) Emission peak broadening versus BODIPY-PC surface concentration (pmol/cm^2) in 16:0-SM or DPPC. The broadening represents the peak width (nm) determined at 50% maximum intensity. Unfilled symbols in panels D, E, and F mark the phase transition region where LE and LC domains coexist.

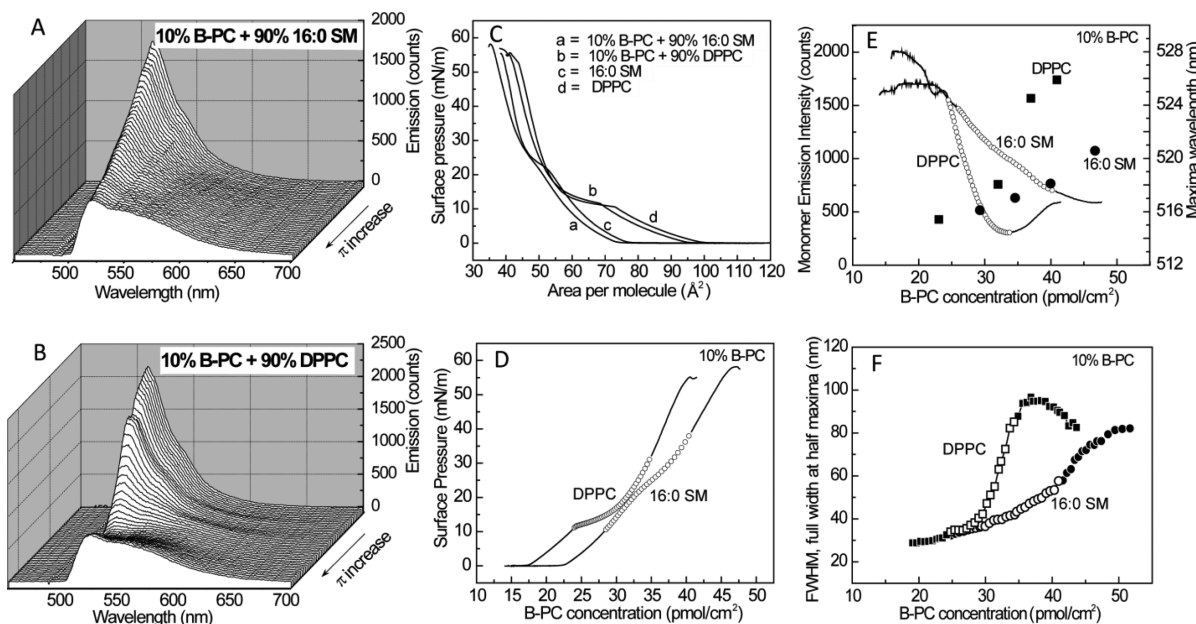


Figure 5. Compression-induced changes in fluorescence emission properties and force–area isotherms for 10 mol % $\text{Me}_4\text{-BODIPY-8-PC}$ mixed with either 16:0-SM or DPPC. (A, B) Representative emission spectra obtained for mixed monolayers of 1 mol % BODIPY-PC and 16:0-SM (A) or DPPC (B). (C) Monolayer isotherms for 16:0-SM and DPPC showing surface pressure versus average molecular area in absence and presence of lipid fluorophore. (D) Surface pressure (π) versus BODIPY-PC surface concentration (pmol/cm^2) response. (E) Monomer emission intensity (solid line) and emission wavelength maximum (λ_{\max}) (symbol) versus BODIPY-PC surface concentration (pmol/cm^2) in 16:0-SM or DPPC. The monomer emission intensity represents the integrated area over the 505–535 nm range. (F) Emission peak broadening versus BODIPY-PC surface concentration (pmol/cm^2) in 16:0-SM or DPPC. The broadening represents the peak width (nm) determined at 50% maximum intensity. Unfilled symbols in panels D, E, and F mark the phase transition region where LE and LC domains coexist.

references therein.) Figures 3C,D show the relationship between surface pressure and $\text{Me}_4\text{-BODIPY-8-PC}$ lateral concentration, i.e. surface density for the two matrix lipids. As

shown by Figure 3E, at 10 mol % $\text{Me}_4\text{-BODIPY-8-PC}$, the monomer (505–535 nm) emission intensities and λ_{\max} apparent red-shifts exhibit linear response patterns but with

stronger changes elicited in 18:1-SM than in POPC. In both cases, the changes are significantly greater in 18:1-SM than in POPC (Figure 3E). In contrast, similar gradual increases in BODIPY emission peak broadness (Figure 3F) occur in both 18:1-SM and POPC. At 20 mol % PC-fluorophore, the response patterns remained similar but were muted compared to those exhibited at 10 mol % due to excessively high self-quenching (data not shown). Overall, the spectral response of Me₄-BODIPY-8-PC is consistent with high miscibility in the fluid-like LE phase of 18:1-SM and POPC albeit minor packing differences that subtly affect fluorophore orientation and lateral distribution.

Me₄-BODIPY-8-PC Response in Dipalmitoylphosphatidylcholine. To determine if changes in lipid phase state, i.e. transition from the fluid-like, liquid-expanded (LE) state to the gel-like, liquid condensed (LC) state, affect the Me₄-BODIPY-8-PC emission signal, fluorescence spectra were collected as DPPC monolayers containing 1 mol % of fluorescent PC were being laterally compressed. Figure 4 shows ~50 samplings from the >500 fluorescence spectra collected during acquisition of each force-area isotherm. Me₄-BODIPY-8-PC emission intensity and peak shape both changed dramatically as a function of increasing PC fluorophore packing density resulting from increasing surface pressure (Figure 4A,B). At low π producing only fluid-like LE phase, the fluorescence intensity was ~50% higher in DPPC than in POPC or 18:1-SM over the same low surface pressure range but also declined slightly with increasing fluorophore surface concentration presumably due to self-quenching (Figures 2E and 4E). At π sufficiently high to induce onset of the DPPC LE/LC phase transition, the Me₄-BODIPY-8-PC emission intensity showed a discontinuity, i.e. dip (Figure 4E). This response could reflect orientational restrictions imposed on the probe or possibly superlattice ordering of the probe distribution in the monolayer.^{52,53} After a slight increase, the intensity declined dramatically as the LE/LC transition midpoint was surpassed. Upon completion of the transition, minimal intensity was observed. Thereafter, the intensity rose slightly when only ordered LC phase existed until the film collapsed. The λ_{max} apparent red-shift also was strongly affected by the LE/LC phase transition of DPPC. At low π when only LE phase existed, the λ_{max} apparent red-shift was similar to that for POPC (Figure 4E). Upon reaching the LE/LC phase transition midpoint, significantly larger λ_{max} apparent red-shift was observed with increasing π . Figure 4F shows that spectral broadening remained relatively unchanged at low π producing fluid-like LE phase and then suddenly began to increase at the surface pressure and fluorophore surface density corresponding to the approximate midpoint of the LE/LC phase transition. Maximum broadening was observed upon completion of the LE/LC phase transition when only gel-like LC phase existed. Further compression of the DPPC LC phase resulted in diminished spectral broadening (Figure 4F). Notably, the preceding dramatic spectral changes were observed with a probe amount (1 mol % Me₄-BODIPY-8-PC) producing no discernible effect on the force-area isotherm or LE/LC phase transition of DPPC (Figure 4C).

To define and better understand the mixing behavior of the PC fluorophore in DPPC, 10 mol % Me₄-BODIPY-8-PC also was studied (Figure 5). Peak intensity and spectral broadening originating from a 560–585 nm shoulder peak were more pronounced (Figure 5B). Minimum peak intensity was observed as DPPC completed the LE/LC phase transition, but the intensity then rose steadily as π increased (Figure 5E).

The response pattern of the λ_{max} apparent red-shift mimicked that of 1% PC-fluorophore but was exacerbated (Figures 4E and 5E). Spectral broadening of 10 mol % lipid fluorophore also mimicked the 1% response in DPPC (Figure 5F). Little change in broadening was observed at low π producing fluid-like LE phase but a sudden increase occurred when the surface pressure and the fluorophore surface density reached the approximate midpoint of the LE/LC phase transition. Maximum broadening was observed upon completion of the LE/LC phase transition when only gel-like LC phase existed and further compression of the DPPC LC phase resulted in strongly diminished spectral broadening (Figure 5E). At 20 mol % BODIPY-PC, the same general patterns were observed as for 10 mol % PC probe but were muted by self-quenching (data not shown).

When present at 10 mol %, Me₄-BODIPY-8-PC exerted a slight condensing effect on DPPC rather than the expected average molecular area expansion because of PC-probe fluid-like LE behavior as a pure entity.¹⁶ The 10 mol % of Me₄-BODIPY-8-PC also slightly elevated the LE/LC transition onset π (Figure 5C). Yet, the LE/LC transition remained sharp even at 20 mol % Me₄-BODIPY-8-PC (not shown). Thus, by classic force-area analyses, hints of partial nonideal mixing were evident for 10 and 20 mol % PC fluorophore, but 1 mol % Me₄-BODIPY-8-PC had no discernible effect on the LE and LC phases of DPPC. Strikingly, changes in fluorescence at all PC probe concentrations indicated nonideal mixing of PC fluorophore between DPPC phases even at low amounts (1 mol %). Taken together, the data suggest that 1 mol % BODIPY-PC is much less miscible in the gel-like LC phase of DPPC (than the fluid-like LE phase) and concentrates in the LE phase and along the domain boundaries when both phases coexist. The tendencies for lipid probes carrying fluorophores on their acyl chains (e.g., 1% probe) to partition to the fluid-like LE phase rather than the gel-like LC phase and to concentrate along domain boundaries in the mixed phase region are common occurrences.^{23–25} Notably, the dramatic spectral changes accompanying the lateral concentrating of 1 mol % Me₄-BODIPY-8-PC in DPPC do not become obvious until the approximate transition midpoint. At this point, the fluid-like LE phase continuum containing dispersed LC phase domains transitions to a gel-like LC phase continuum containing dispersed LE phase domains, and the signal intensity and broadening begin to change in dramatic fashion. Under packing conditions when only LC phase exists for DPPC, Me₄-BODIPY-PC mixing into the tight DPPC lattice is energetically unfeasible, leading the PC probe to be excluded. Even at low concentration (1 mol %) in the DPPC LC phase, Me₄-BODIPY-8-PC molecules appear to segregate and form clusters that could impose conformational restrictions to the probe aggregate/dimer. In the clusters, the local probe concentration is high and excited state dimer emission keeps spectral intensity broadened compared to the DPPC LE phase.

Our conclusions arise from current understanding of BODIPY photophysical behavior. Dilute noninteracting BODIPY monomers exhibit an emission peak centered in the 506–515 nm range.^{15,16,18,26–31} In contrast, additional absorption and emission peaks occur at high BODIPY concentrations, reflecting dimer emission and resonance energy transfer (Förster distance = 57 Å) to transient ground state dimers that partially quench monomer emission. Emission from ground-state BODIPY dimers, denoted D_{II} (J-dimer), occurs when BODIPY rings orient in planar fashion with their S₀ → S₁

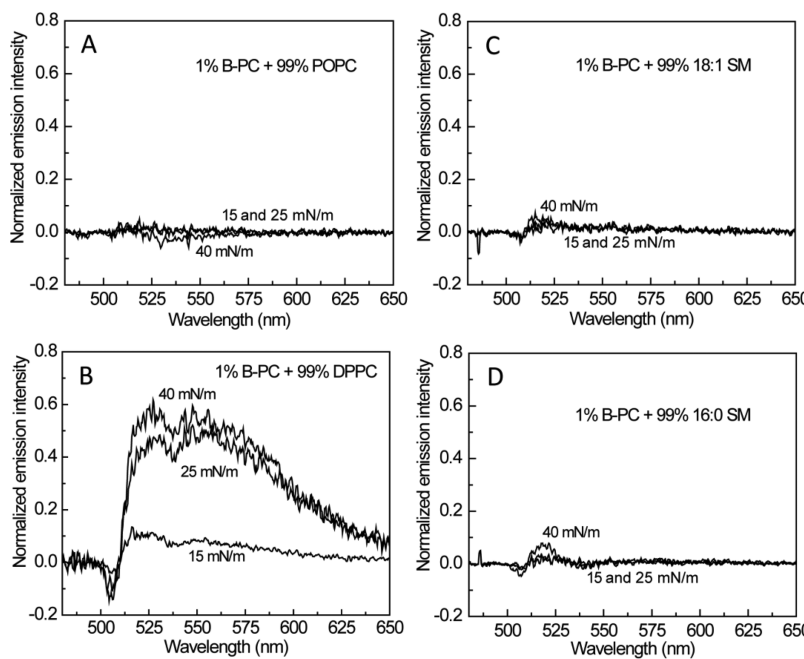


Figure 6. Evaluation of surface concentration-dependent dimer emission by 1 mol % $\text{Me}_4\text{-BODIPY-8-PC}$ in different monolayer matrices using normalized difference spectra. The normalized emission peak obtained at 5 mN/m (= monomer) was subtracted from spectra obtained at 15, 25, and 40 mN/m for each matrix lipid. (A) POPC; (B) DPPC; (C) 18:1-SM; (D) 16:0-SM. The inflection depth at ~ 510 nm reflects the magnitude of the λ_{\max} apparent red-shift. The normalized spectra used to produce the difference spectra are shown in Figure S1. Similar comparisons at 10 mol % $\text{Me}_4\text{-BODIPY-8-PC}$ are presented in Figures S2 and S3.

transition dipoles aligned at $\sim 55^\circ$. Typically, the D_{II} emission peak reflects energy transfer from excited-state monomers to the ground-state D_{II} dimers, which absorb near 570 nm and emit near 630 nm.²⁶ BODIPY rings also can undergo sandwich-like stacking and parallel alignment of the transition dipoles to form ground-state dimers referred to as D_I (H-dimer). Absorption occurs near 477 nm but produces no fluorescence emission after excitation.^{29,30} Tetramethylated BODIPY ($\text{Me}_4\text{-BODIPY-8-PC}$) exhibits an emission shoulder (~ 570 nm) at high surface concentrations¹⁶ but no trace of the 620–630 nm peak characteristic of dimethyl-BODIPY dimer. The emission shoulder at ~ 570 nm appears to be consistent with energy transfer between excited state monomer and transient ground state dimers aligned differently than D_{II} dimers.^{29,30} What is clear is that much of the monomer emission peak intensity becomes dampened by relaxation processes (nonfluorescent) as intensity is less than expected at 10 mol % compared to 1 mol % as well as at 20 mol % compared to 10 mol % PC-probe.

$\text{Me}_4\text{-BODIPY-8-PC}$ Response in 16:0 SM. To determine if $\text{Me}_4\text{-BODIPY-8-PC}$ exhibits lateral mixing differences in naturally predominant SM species compared to DPPC, fluorescence spectra were collected while 16:0-SM monolayers containing 1 mol % fluorescent PC were being laterally compressed (Figure 4). A strikingly different intensity pattern for $\text{Me}_4\text{-BODIPY-8-PC}$ emission is observed in 16:0 SM compared to DPPC with increasing PC fluorophore packing density resulting from increasing surface pressure (Figure 4A,B). When fluid-like LE phase exists ($\pi < 22$ mN/m; density $< \sim 3$ pmol/cm²), the emission intensity initially is only slightly higher in 16:0-SM than in DPPC and gradually decreases. A discontinuity in the intensity profile occurs with the onset of the LE/LC phase transition (Figure 4E) as with DPPC. However, in 16:0-SM, the intensity remains nearly unchanged throughout the LE/LC transition before declining dramatically

and almost linearly when the transition nears completion (Figure 4E). The response contrasts that in DPPC where the dramatic decline in lipid probe intensity begins approximately midway through the LE/LC transition, reaches a minimum upon completion of the transition, and then increases until film collapse. The differing onset points for intensity decline in 16:0-SM and DPPC appear to reflect persistence of stable LC domains formed by 16:0-SM until the transition is nearly completed. The resistance to formation of a LC phase continuum by 16:0-SM would keep domain boundaries intact where the lipid fluorophore probe can remain relatively well dispersed. Our explanation is supported by fluorescence imaging showing multilobed, leaf-like LC domains (6-fold symmetry) formed by SM compared to less intricate S-shaped and trilobed LC domains of DPPC.^{32–34} Although only slightly smaller in size, the more intricate morphology of the SM domains results in significantly more phase boundary than for DPPC domains. Remarkably, the SM domains resist coalescence even when very high surface pressures are applied to force coalescence with each other.³² This response presumably reflects higher long-range repulsive dipole–dipole interactions counteracting the line tension effect that drives domains toward less intricate circular morphologies.³⁵ It is also noteworthy that the responses of the λ_{\max} apparent red-shift and the peak broadness for 16:0 SM (Figure 4E,F) more closely resemble those observed in 18:1 SM and POPC rather than of DPPC. Overall, the data suggest that $\text{Me}_4\text{-BODIPY-8-PC}$ (1 mol %) miscibility in 16:0 SM remains high regardless of 16:0 SM phase state, in contrast to DPPC where exclusion from the DPPC LC phase occurs.

At higher $\text{Me}_4\text{-BODIPY-8-PC}$ content (10 mol %), the lipid probe intensity response, the spectral broadening, and the force–area isotherms (Figure 5) indicated effects exerted by the lipid probe itself in the 16:0-SM and DPPC matrices. The

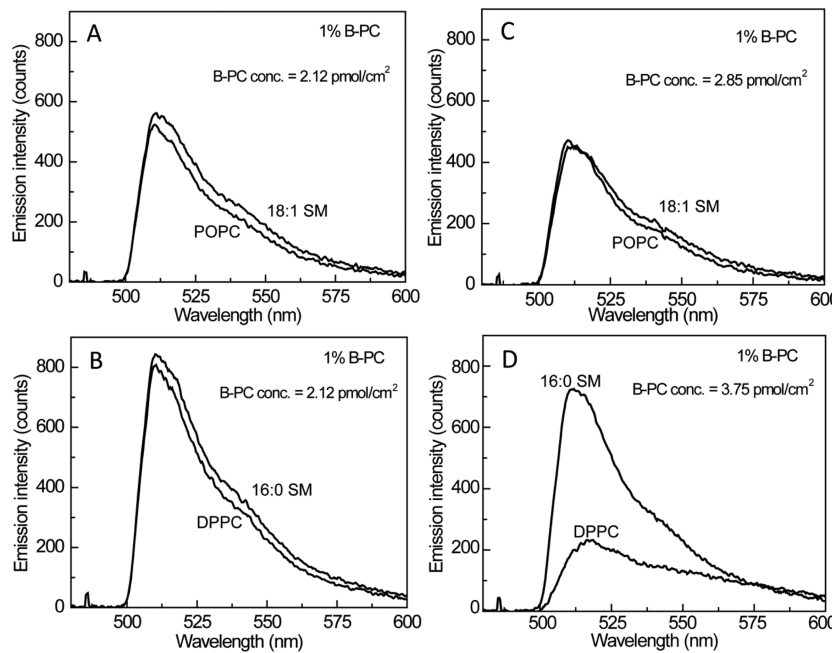


Figure 7. Spectra for 1 mol % $\text{Me}_4\text{-BODIPY-8-PC}$ in different monolayer matrices compared at identical interfacial molecular packing areas. (A) POPC and 18:1-SM at $78 \text{ \AA}^2/\text{molecule}$ ($\text{Me}_4\text{-BODIPY-8-PC} = 2.12 \text{ pmol}/\text{cm}^2$); (B) DPPC and 16:0-SM at $78 \text{ \AA}^2/\text{molecule}$ ($\text{Me}_4\text{-BODIPY-8-PC} = 2.12 \text{ pmol}/\text{cm}^2$); (C) POPC and 18:1-SM at $58 \text{ \AA}^2/\text{molecule}$ ($\text{Me}_4\text{-BODIPY-8-PC} = 2.85 \text{ pmol}/\text{cm}^2$); (D) DPPC and 16:0-SM at $45 \text{ \AA}^2/\text{molecule}$ ($\text{Me}_4\text{-BODIPY-8-PC} = 3.75 \text{ pmol}/\text{cm}^2$).

effects included a damped LE/LC phase transition in 16:0-SM that was not evident in DPPC. At 20% $\text{Me}_4\text{-BODIPY-8-PC}$, the same general pattern persisted (data not shown), but the spectral broadening was magnified by the dominance of the shoulder peak in the 550–580 nm spectral region. The spectral broadening produced by 10 and 20 mol % $\text{Me}_4\text{-BODIPY-8-PC}$ was expected because of the higher surface density of the lipid fluorophore and resulting increase in excited state dimer emission.

Additional support for the miscibility of the PC-fluorophore in 16:0-SM monolayers was provided by force-area isotherms. As with DPPC, the presence of 1 mol % PC fluorophore had almost no effect on the force-area isotherm of 16:0-SM (Figure 4B,C). At 10 mol % $\text{Me}_4\text{-BODIPY-8-PC}$ exerted a slight condensing effect on 16:0-SM as also observed for DPPC (Figure 5C). The 10 mol % $\text{Me}_4\text{-BODIPY-8-PC}$ slightly elevated the onset surface pressure and decreased the sharpness of the LE/LC transition and decreased isotherm slopes of LC phase (16:0-SM) consistent with enhanced lateral elasticity.

As a final check, the $\text{Me}_4\text{-BODIPY-8-PC}$ emission spectra (1 mol %) for each lipid matrix were compared in two additional ways. We evaluated for the presence of an excited state dimer emission peak at various surface pressures including high surface pressure that mimics biomembranes packing conditions (e.g., $\pi = 40 \text{ mN}/\text{m}$) by subtraction of the monomer spectrum. Figure 6 shows the lack of an excited state dimer peak for 1 mol % $\text{Me}_4\text{-BODIPY-8-PC}$ in POPC, 18:1-SM, and 16:0-SM, a finding consistent with relatively high miscibility of the PC fluorophore. In contrast, with DPPC (Figure 6B), excited state dimer peaks were clearly evident at 25 and 40 mN/m , indicating exclusion from the gel-like LC phase, but not at low pressure (15 mN/m) when fluid-like LE phase exists in the LE/LC transition region. Notably, negligible excited state dimer peak was detected in 16:0-SM at 40 mN/m , a pressure also yielding LC phase. To show that formation of the excited state

dimer peak depended on increased $\text{Me}_4\text{-BODIPY-8-PC}$ surface concentration, the same analysis was repeated for each lipid matrix but at 10 mol % PC-fluorophore (Figure S2). The presence of excited state dimer peaks is evident in all lipid matrices, but of much lesser magnitude in POPC, 18:1-SM, and 16:0-SM compared to DPPC. The normalized spectra used to generate Figure 6 and Figure S2 are provided in Figures S1 and S3.

Because $\text{Me}_4\text{-BODIPY-8-PC}$ emission is responsive to surface concentration, we also compared spectra obtained in each lipid matrix at identical mean molecular areas. Figures 7A and 7B show the similar spectral responses for 18:1-SM and POPC monolayers as well as those for 16:0-SM and DPPC, respectively, all acquired at $78 \text{ \AA}^2/\text{molecule}$. Since this packing area yields fluid, LE state for all four lipids as well as identical $\text{Me}_4\text{-BODIPY-8-PC}$ surface concentrations of $2.12 \text{ pmol}/\text{cm}^2$, we suggest that the moderately differing intensities reflect acyl chain structural differences (*cis* 9–10 unsaturated vs saturated) that affect the average orientation of the BODIPY fluorophore intercalated among lipid chains in the monolayer. Figures 7C and 7D show the same lipids, but at higher lipid packing densities that mimic the bilayer situation. Again, similar emission responses are observed for POPC and 18:1-SM (Figure 7C) at molecular areas of 58 \AA^2 , which is near the collapse areas ($\sim 55 \text{ \AA}^2$) of their fluid LE films. In contrast, markedly different emission responses are observed for DPPC and 16:0-SM (Figure 7D) at molecular areas of 45 \AA^2 , which yields LC films and $\text{Me}_4\text{-BODIPY-8-PC}$ surface concentrations of $3.75 \text{ pmol}/\text{cm}^2$. Notably, the emission response in 16:0-SM is rather similar to that observed at lower packing density (Figure 7B). Altogether, our findings are consistent with the seemingly counterintuitive outcome of PC fluorophore mixing better with the LC phase of 16:0-SM compared to LC phase of DPPC as well as being only moderately less miscible with the

SM LC phase than the SM LE phase but poorly miscible with DPPC LC phase.

SM and PC Structural Differences That Affect Their Phase Behavior. To understand how the preceding experimental responses could arise, it is useful to examine structural features that distinguish SM from PC and that likely to contribute to the intriguing physiochemical behavior of SM. While SM and PC both share the zwitterionic polar headgroup, phosphocholine, and have two long nonpolar hydrocarbon chains, they differ with respect to the type of linkage between the long chains and the backbone. As pointed out earlier, in naturally occurring PC, both hydrocarbon chains are ester-linked to a glycerol backbone, the *sn*-1 chain usually is saturated (e.g., palmitate or stearate), while the *sn*-2 chain generally contains one or more *cis* double bonds. In contrast, in SM, the sphingoid base serves the dual role as both the interfacial backbone and nonpolar hydrocarbon chain and the single acyl chain is amide-linked and tends to be saturated. The initial three carbons of the 18-carbon sphingoid base of SM are configurationally analogous to the glycerol backbone of PC. The remaining 15 carbons of the sphingoid base resemble the saturated palmitoyl *sn*-1 chain of DPPC. The *sn*-2 acyl chain of DPPC and the *N*-linked acyl chain of SM share a similar conformation in that their first two carbons extend roughly parallel to the bilayer interface, but the chains then bend sharply to become aligned with the respective *sn*-1 acyl chain or sphingoid base.^{14,36–38} The resulting axial displacement leads to positional inequivalence of the carbon atoms along the two adjacent intramolecular chains.

Despite the preceding similarities in general conformation and shape, the sphingoid chain of SM possesses a 3-hydroxyl group and a 4,5 *trans* double bond that affect hydration and hydrogen bonding with surrounding water and/or neighboring lipids. For instance, SM and PC produce distinct ³¹P NMR resonances and Pr³⁺ induces a larger downfield shift for SM than for PC, consistent with their phosphate groups residing in nonidentical local environments.^{39,40} Also, the quaternary ammonium headgroup is more rigid in SM than in PC as indicated by ¹⁴N NMR and ¹³C/¹H CP-MAS NMR.^{41,42} SMs in monolayers at biomembrane-like packing conditions have smaller cross-sectional molecular areas than their respective chain-matched PCs (ref 42 and references therein). *In silico* modeling by molecular dynamics simulations also predicts smaller molecular cross-sectional area and volume in fluid phase bilayers for *N*-palmitoyl SM than for DPPC.^{43,44}

The unique contribution of the 4,5-*trans* double bond in regulating the interfacial dipole potential, lateral elasticity, and molecular packing of sphingolipids is clear from monolayer studies of different ceramide analogues.⁴⁵ The key roles played by the 4,5-*trans* double bond and the 3-OH group in organizing interfacial water and mediating intramolecular hydrogen bonds via strongly bound water molecules also are indicated by solution NMR studies^{46,47} and molecular dynamics simulations^{43,44} of SM and dihydro-SM (DHSM), which lacks the 4,5 *trans* double bond. Elimination of the 4,5-*trans* double bond modifies the hydration of the interfacial region, distorts hydrogen bond interactions, and affects the 3-hydroxy group conformation in ways that increase molecular packing density and alter the molecular dipole potential.^{21,42,48} The changes are manifested in the overall interaction between phosphocholine and its subtending ceramide moiety. In SM, intramolecular hydrogen bonding involving bridging water molecules occurs between the 3-OH group of the sphingoid base and the bridge

oxygen of phosphate.^{39,42,47} In DHSM, this intramolecular hydrogen bonding is disrupted, increasing phosphocholine conformational flexibility and enabling DHSM with saturated acyl chains to undergo tighter lateral packing.^{21,42,48,49} Thus, the presence of the 4,5 *trans* double bond in SM generates gel phase packing that differs from DHSM or DPPC. Direct support for this idea comes not only from NMR studies of SM bilayers⁴² but also from X-ray diffraction studies of SM monolayers that reveal almost no molecular tilt compared to DPPC ($\sim 30^\circ$) at high surface pressures and show the SM LC phase lacking the long-range, in-plane order that characterizes the liquid condensed monolayer phases of PCs and PAs with saturated acyl chains.⁵⁰ The SM molecules appear to be locked into tightly packed, irregular positions that promote a glassy, amorphous packing state rather than a more crystalline state for the chains. Indeed, the amorphously packed LC state of SM is known to display elevated cohesive strength and improved resilience,^{20,21} presumably by avoiding formation of rigid grain boundaries and dislocations that weaken crystalline materials. Molecular dynamics modeling of this packing state shows the headgroup and immediately adjacent chain regions to be denser, i.e., have fewer packing voids, in SM than DPPC.⁵¹ This tighter packing of the SM interfacial region can be attributed to both intra- and intermolecular hydrogen bonding. The intramolecular hydrogen bonding produces a more upright phosphocholine headgroup relative to the bilayer (or monolayer) surface while the intermolecular hydrogen bonding involving its sphingoid 3-OH group and amide-linkage enhances intermolecular cohesion. The resulting “noose-like” tightening at the SM interfacial region increases density voids of all sizes toward the bilayer center, a feature expected to facilitate accommodation and promote better mixing with acyl-labeled PCs carrying a slightly bulky BODIPY ω -linked to the acyl chain. From a broader biological perspective, a membrane region (e.g., microdomain) containing a higher density of packing voids toward the bilayer center also could serve as a localization site favored by certain peptides and proteins that need deeper embedding in membranes to function optimally. The unique properties of SM gel phase (compared to DPPC) appear to be well-suited for such a role despite the phase transition temperature of SM being above physiological temperature. Because of the important role played by SM in raft microdomain formation, we are currently using this new monolayer fluorescence platform to compare the accommodation of cholesterol by the condensed (gel) phases of SM and DPPC.

CONCLUSIONS

In the present study, we have relied on the concentration-dependent emission changes of Me₄-BODIPY-8-PC induced by monolayer lateral compression to evaluate nanoscale alterations in lipid packing and phase state of SM and PC with identical acyl chains. Slightly better mixing of Me₄-BODIPY-8-PC with the fluid-like, liquid expanded phase of 1-palmitoyl-2-oleoyl-PC is observed compared to *N*-oleoyl-SM. Remarkably, in the gel-like, liquid condensed phase, Me₄-BODIPY-8-PC mixes better with *N*-palmitoyl-SM than dipalmitoyl-PC, consistent with naturally abundant SMs with saturated acyl chains forming gel-like lipid phase(s) with enhanced ability to accommodate deeply embedded components compared to dipalmitoyl-PC gel phase. The findings reveal a fundamental difference in the lateral packing properties of SM and PC that occurs even when their acyl chains match.

■ ASSOCIATED CONTENT

● Supporting Information

Figures S1–S3. This material is available free of charge via the Internet at <http://pubs.acs.org>.

■ AUTHOR INFORMATION

Corresponding Authors

*E-mail: hlbroc@hi.umn.edu (H.L.B.).

*E-mail: jgmol@ibch.ru (J.G.M.).

*E-mail: reb@umn.edu (R.E.B.).

Notes

The authors declare no competing financial interest.

■ ACKNOWLEDGMENTS

We gratefully acknowledge the support of NIH/NIGMS 45928, NIH/NHLBI 49180, Russian Foundation for Basic Research Grant #12-04-00168, and the Hormel Foundation.

■ REFERENCES

- (1) van Meer, G.; Voelker, D. R.; Feigenson, G. W. Membrane Lipids: Where They Are and How They Behave. *Nat. Rev. Mol. Cell Biol.* **2008**, *9*, 112–124.
- (2) Goñi, F. M.; Alonso, A.; Bagatolli, L. A.; Brown, R. E.; Marsh, D.; Prieto, M.; Thewalt, J. L. Phase Diagrams of Lipid Mixtures Relevant to the Study of Membrane Rafts. *Biochim. Biophys. Acta* **2008**, *1781*, 665–684.
- (3) Simons, K.; Gerl, M. J. Revitalizing Membrane Rafts: New Tools and Insights. *Nat. Rev. Mol. Cell Biol.* **2010**, *11*, 688–699.
- (4) Lingwood, D.; Simons, K. Lipid Rafts as a Membrane Organizing Principle. *Science* **2010**, *327*, 46–50.
- (5) Stottrup, B. L.; Nguyen, A. H.; Tüzel, E. Taking Another Look with Fluorescence Microscopy: Image Processing Techniques in Langmuir Monolayers for the Twenty-First Century. *Biochim. Biophys. Acta* **2010**, *1798*, 1289–1300.
- (6) Fanani, M. L.; Hartel, S.; Maggio, B.; De Tullio, L.; Jara, J.; Olmos, F.; Oliveira, R. G. The Action of Sphingomyelinase in Lipid Monolayers as Revealed by Microscopic Image Analysis. *Biochim. Biophys. Acta* **2010**, *1798*, 1309–1323.
- (7) Huang, B.; Bates, M.; Zhuang, X. Super-Resolution Fluorescence Microscopy. *Annu. Rev. Biochem.* **2009**, *78*, 993–1016.
- (8) Schermelleh, L.; Heintzmann, R.; Leonhardt, H. A Guide to Super-Resolution Fluorescence Microscopy. *J. Cell Biol.* **2010**, *190*, 165–175.
- (9) Möhwald, H. Phospholipid Monolayers. In *Handbook of Biological Physics*; Lipsky, R., Sackmann, E., Eds.; Elsevier Science: Amsterdam, 1995; Vol. 1, pp 161–211.
- (10) Brockman, H. L. Lipid Monolayers: Why Use Half a Membrane to Characterize Protein-Membrane Interactions? *Curr. Opin. Struct. Biol.* **1999**, *9*, 438–443.
- (11) Brezesinski, G.; Möhwald, H. Langmuir Monolayers to Study Interactions at Model Membrane Surfaces. *Adv. Colloid Interface Sci.* **2003**, *100*, 563–584.
- (12) Zhai, X.; Li, X.-M.; Momsen, M. M.; Brockman, H. L.; Brown, R. E. Lactosylceramide: Lateral Interactions with Cholesterol. *Biophys. J.* **2006**, *91*, 2490–2500.
- (13) Brown, R. E.; Brockman, H. L. Using Monomolecular Films to Characterize Lipid Lateral Interactions. *Methods Mol. Biol.* **2007**, *398*, 41–58.
- (14) Brown, R. E. Sphingolipid Organization in Biomembranes: What Physical Studies of Model Membranes Reveal. *J. Cell Sci.* **1998**, *111*, 1–9.
- (15) Dahim, M.; Mizuno, N. K.; Li, X.-M.; Momsen, W. E.; Momsen, M. M.; Brockman, H. L. Physical and Photophysical Characterizations of a BODIPY Phosphatidylcholine as a Membrane Probe. *Biophys. J.* **2002**, *83*, 1511–1524.
- (16) Boldyrev, I. A.; Zhai, X.; Momsen, M. M.; Brockman, H. L.; Brown, R. E.; Molotkovsky, J. G. New BODIPY Lipid Probes for Fluorescence Studies of Membranes. *J. Lipid Res.* **2007**, *48*, 1518–1532; and errata: *J. Lipid Res.* **2007**, *48*, 1900.
- (17) Boldyrev, I. A.; Molotkovsky, J. G. A Synthesis and Properties of New 4,4-Difluoro-3a,4a-Diaza-s-Indacene (BODIPY)-Labeled Lipids. *Russ. J. Bioorg. Chem.* **2006**, *32*, 78–83.
- (18) Sugar, I. P.; Zhai, X.; Boldyrev, I. A.; Momsen, M. M.; Molotkovsky, J. G.; Brockman, H. L.; Brown, R. E. Characterization of the Lateral Distribution of Fluorescent Lipid in Binary-Constituent Lipid Monolayers by Principal Component Analysis. *Int. J. Biomed. Imaging* **2010**, e125850.
- (19) Maulik, P. R.; Shipley, G. G. N-Palmitoyl Sphingomyelin Bilayers: Structure and Interactions with Cholesterol and Dipalmitoylphosphatidylcholine. *Biochemistry* **1996**, *35*, 8025–8034.
- (20) Li, X.-M.; Smaby, J. M.; Momsen, M. M.; Brockman, H. L.; Brown, R. E. Sphingomyelin Interfacial Behavior: The Impact of Changing Acyl Chain Composition. *Biophys. J.* **2000**, *78*, 1921–1931.
- (21) Kuikka, M.; Ramstedt, B.; Ohvo-Rekila, H.; Tuuf, J.; Slotte, J. P. Membrane Properties of D-erythro-N-Acyl Sphingomyelins and their Corresponding Dihydro Species. *Biophys. J.* **2001**, *80*, 2327–2337.
- (22) Slotte, J. P. Molecular Properties of Various Structurally Defined Sphingomyelins – Correlation of Structure with Function. *Prog. Lipid Res.* **2013**, *52*, 206–219.
- (23) Vaz, W. L. C.; Melo, E. Fluorescence Spectroscopic Studies on Phase Heterogeneity in Lipid Bilayer Membranes. *J. Fluoresc.* **2001**, *11*, 255–271.
- (24) Honigmann, A.; Walter, C.; Erdmann, F.; Eggeling, C.; Wagner, R. Characterization of Horizontal Lipid Bilayers as a Model System to Study Lipid Phase Separation. *Biophys. J.* **2010**, *98*, 2886–2894.
- (25) Jorgensen, K.; Ipsen, J. H.; Mouritsen, O. G.; Bennet, D.; Zuckermann, M. J. A General Model for the Interaction of Foreign Molecules with Lipid Membranes: Drugs and Anaesthetics. *Biochim. Biophys. Acta* **1991**, *1062*, 227–238.
- (26) Karolin, J.; Johansson, L.B.-Å.; Strandberg, L.; Ny, T. Fluorescence and Absorption Spectroscopic Properties of Dipyrrometheneboron Difluoride (BODIPY) Derivatives in Liquids, Lipid Membranes, and Proteins. *J. Am. Chem. Soc.* **1994**, *116*, 7801–7806.
- (27) Mikhalyov, I.; Bogen, S.-T.; Johansson, L. B.-Å. Donor-Donor Energy Migration (DDEM) as a Tool for Studying Aggregation in Lipid Phases. *Spectrochim. Acta, Part A* **2001**, *57*, 1839–1845.
- (28) Mikhalyov, I.; Gretskaya, N.; Bergström, F.; Johansson, L. B.-Å. Electronic Ground and Excited State Properties of Dipyrrometheneboron Difluoride (BODIPY): Dimers with Application to Biosciences. *Phys. Chem. Chem. Phys.* **2002**, *4*, 5663–5670.
- (29) Bergström, F.; Mikhalyov, I.; Häggglöf, P.; Wortmann, R.; Ny, T.; Johansson, L.B.-Å. Dimers of Dipyrrometheneboron Difluoride (BODIPY) with Light Spectroscopic Applications in Chemistry and Biology. *J. Am. Chem. Soc.* **2002**, *124*, 196–204.
- (30) Tleugabulova, D.; Zhang, Z.; Brennan, J. D. Characterization of BODIPY Dimers Formed in a Molecularly Confined Environment. *J. Phys. Chem. B* **2002**, *106*, 13133–13138.
- (31) Loudet, A.; Burgess, K. BODIPY Dyes and Their Derivatives: Syntheses and Spectroscopic Properties. *Chem. Rev.* **2007**, *107*, 4891–4932.
- (32) Prenner, E.; Honsek, G.; Dirk Höning, D.; Möbius, D.; Lohner, K. Imaging of the Domain Organization in Sphingomyelin and Phosphatidylcholine Monolayers. *Chem. Phys. Lipids* **2007**, *145*, 106–118.
- (33) Slotte, J. P.; Mattjus, P. Visualization of Lateral Phases in Cholesterol and Phosphatidylcholine Monolayers at the Air/Water Interface – A Comparative Study with Two Different Reporter Molecules. *Biochim. Biophys. Acta* **1995**, *1254*, 22–29.
- (34) Brewer, J.; de la Serna, J. B.; Wagner, K.; Bagatolli, L. A. Multiphoton Excitation Fluorescence Microscopy in Planar Membrane Systems. *Biochim. Biophys. Acta* **2010**, *1798*, 1301–1308.
- (35) McConnell, H. M.; de Koker, R. Equilibrium Thermodynamics of Lipid Monolayer Domains. *Langmuir* **1996**, *12*, 4897–4904.

- (36) Li, X.-M.; Momsen, M. M.; Smaby, J. M.; Brockman, H. L.; Brown, R. E. Cholesterol Decreases the Interfacial Elasticity and Detergent Solubility of Sphingomyelins. *Biochemistry* **2001**, *40*, 5954–5963.
- (37) Pascher, I.; Lundmark, M.; Nyholm, P.-G.; Sundell, S. Crystal Structure of Membrane Lipids. *Biochim. Biophys. Acta* **1992**, *113*, 339–373.
- (38) Mehnert, T.; Jacob, K.; Bittman, R.; Beyer, K. Structure and Lipid Interaction of N—PalmitoylSphingomyelin in Bilayer Membranes as Revealed by ^2H -NMR Spectroscopy. *Biophys. J.* **2006**, *90*, 939–946.
- (39) Schmidt, C. F.; Barenholz, Y.; Thompson, T. E. A Nuclear Magnetic Resonance Study of Sphingomyelin in Bilayer Systems. *Biochemistry* **1977**, *16*, 2649–56.
- (40) Malewicz, B.; Valiyaveettil, J. T.; Jacob, K.; Byun, H.-S.; Mattjus, P.; Baumann, W. J.; Bittman, R.; Brown, R. E. The 3-Hydroxy Group and 4,5-trans Double Bond of Sphingomyelin are Essential for Modulation of Galactosylceramide Transmembrane Asymmetry. *Biophys. J.* **2005**, *88*, 2670–2680.
- (41) Siminovitch, D. J.; Jeffery, K. R. Orientational Order in the Choline Headgroup of Sphingomyelin: A ^{14}N -NMR Study. *Biochim. Biophys. Acta* **1981**, *645*, 270–278.
- (42) Bruzik, K. S.; Sobon, B.; Salamonczyk, G. M. Nuclear Magnetic Resonance Study of Sphingomyelin Bilayers. *Biochemistry* **1990**, *29*, 4017–4021.
- (43) Mombelli, E.; Morris, R.; Taylor, W.; Fratermali, F. Hydrogen-Bonding Propensities of Sphingomyelin in Solution and in a Bilayer Assembly: A Molecular Dynamics Study. *Biophys. J.* **2003**, *84*, 1507–1517.
- (44) Niemelä, P.; Hyvönen, M. T.; Vattulainen, I. Structure and Dynamics of Sphingomyelin Bilayer: Insight Gained Through Systematic Comparison to Phosphatidylcholine. *Biophys. J.* **2004**, *87*, 2976–2989.
- (45) Brockman, H. L.; Momsen, M. M.; Brown, R. E.; He, L.; Chun, J.; Byun, H.-S.; Bittman, R. The 4,5-Double Bond of Ceramide Regulates its Dipole Potential, Elastic Properties, and Packing Behavior. *Biophys. J.* **2004**, *87*, 1722–1731.
- (46) Ferguson-Yankey, S. R.; Borchman, D.; Taylor, K. G.; DuPre, D. B.; Yappert, M. C. Conformational Studies of Sphingolipids by NMR Spectroscopy. I. Dihydrosphingomyelin. *Biochim. Biophys. Acta* **2000**, *1467*, 307–325.
- (47) Talbott, C. M.; Vorobyov, I.; Borchman, D.; Taylor, K. G.; DuPre, D. B.; Yappert, M. C. Conformational Studies of Sphingolipids by NMR Spectroscopy. II. Sphingomyelin. *Biochim. Biophys. Acta* **2000**, *1467*, 326–337.
- (48) Yappert, M. C.; Borchman, D. Sphingolipids in Human Lens Membranes: An Update on their Composition and Possible Biological Implications. *Chem. Phys. Lipids* **2004**, *129*, 1–20.
- (49) Nyholm, T. K. M.; Nylund, M.; Slotte, J. P. A Calorimetric Study of Binary Mixtures of Dihydrosphingomyelin and Sterols, Sphingomyelin, or Phosphatidylcholine. *Biophys. J.* **2003**, *84*, 3138–3146.
- (50) Vaknin, D.; Kelley, M. S. Sphingomyelin at the Air-Water Interface. *J. Chem. Phys.* **2001**, *115*, 7697–7704.
- (51) Kupiainen, M.; Falck, E.; Ollila, S.; Niemelä, P.; Gurtovenko, A. A.; Hyvönen, M. T.; Patra, M.; Karttunen, M.; Vattulainen, I. Free Volume Properties of Sphingomyelin, DMPC, DPPC, and PLPC Bilayers. *J. Comput. Theoret. Nanosci.* **2005**, *2*, 401–413.
- (52) Somerharju, P.; Virtanen, J. A.; Cheng, K. H.; Hermansson, M. The Superlattice Model of Lateral Organization of Membranes and its Implications on Membrane Lipid Homeostasis. *Biochim. Biophys. Acta* **2009**, *1788*, 12–23.
- (53) Chong, P. L.-G.; Zhu, W.; Venegas, B. On the Lateral Structure of Model Membranes Containing Cholesterol. *Biochim. Biophys. Acta* **2009**, *1788*, 2–11.